Journal of Alloys and Compounds 513 (2012) 80–85

Contents lists available at SciVerse ScienceDirect

Journal of Alloys and Compounds

journal homepage: www.elsevier.com/locate/jallcom

Influence of Nd^{3+} substitution on structural, electrical and magnetic properties of nanocrystalline nickel ferrites

T.J. Shinde [a,*], A.B. Gadkari [b], P.N. Vasambekar [c]

[a] Department of Physics, K.R.P. Kanya Mahavidyalaya Islampur 415 409, India
[b] Department of Physics, G.K.G. College Kolhapur 416 012, India
[c] Department of Electronics, Shivaji University Kolhapur 416 004, India

ARTICLE INFO

Article history:
Received 4 October 2010
Received in revised form
28 September 2011
Accepted 2 October 2011
Available online 8 October 2011

Keywords:
Nanostructured materials
Precipitation
Crystal structure
Electrical transport
Magnetic measurements

ABSTRACT

Polycrystalline ferrite samples of $NiNd_xFe_{2-x}O_4$ (where $x = 0$, 0.01, 0.02, and 0.03) system were synthesized by oxalate co-precipitation method and characterized by XRD, IR and SEM techniques. X-ray diffraction analysis confirmed the formation of single phase cubic spinel structure. The lattice constant of all the samples found to increase with increase in Nd^{3+} content. Crystallite size of the samples lies in the range 29.8–31 nm. Infrared spectra show two strong absorption bands in the frequency range 400–600 cm^{-1}, which were respectively attributed to tetrahedral and octahedral sites of the spinel. DC electrical resistivity of Nd^{3+} substituted nickel ferrites is higher than nickel ferrite. Saturation magnetization of the samples increases with increase in Nd^{3+}content.

1. Introduction

Nickel ferrite is technologically important magnetic material extensively used in high frequency applications such as microwave device due to its high resistivity and sufficiently low losses [1]. Electrical and magnetic properties of the ferrites are dependent on method of preparation [2] and the type of substitution [3]. Preparation of ferrites by classical solid state reaction requires a high calcination temperature. This method suffers from disadvantages like chemical inhomogeneity, coarser particle size and impurity insertion during the process [4]. In recent years several researchers have prepared nanosized ferrites by sol–gel method [2,5], emulsion method [6], co-precipitation method [2,7], citrate precursor method [8], tartrate precursor method [9], hydrothermal method [10], reverse micelle technique [11], microemulsions [12], high energy ball milling technique [13] and pulsed wire discharge method [14]. There are many reports in literature on the studies of Ni–Cr [15], Ni–Ge [16], Ni–Zn [17,18], Ni–Al [19], Ni–Cd [20], Ni–Li [21], Ni–Cu [22], Ni–Mg [23] and Ni–Mn [24] ferrites.

Nowadays an important modification in both electrical and magnetic properties is obtained by introducing small amount of foreign ions such as rare earths. This is because the rare earth ions play an important role in determining the magneto crystalline anisotropy in the 4f–3d intermetallic compounds [25,26]. Rezlescu et al. [27] reported that the small substitution of Fe ions by rare earths may favourably influence the magnetic and electrical properties of Ni–Zn ferrites. The effect of lanthanum substitution for iron on the structural and magnetic properties of nickel ferrite has been studied by Al Angari [28]. He found that the lattice parameter, X-ray density and crystallite size increases whereas saturation magnetization decreases with increasing La content. The influence of Y^{3+} substitution on the structural, electrical and dielectric properties of nickel ferrite was reported by Ishaque et al. [29].

The aim of the present work is to investigate the effect of Nd^{3+} ions substitution for Fe^{3+} ions on structural, electrical and magnetic properties of nickel ferrite.

2. Experimental details

Ferrite samples with general formula $NiNd_xFe_{2-x}O_4$ ($x = 0$, 0.01, 0.02 and 0.03) were prepared by oxalate co-precipitation method. The AR grade nickel sulphate (Thomas Baker), ferrous sulphate (Thomas Baker) and neodymium sulphate (Alfa Aesar) were weighed in required proportions and dissolved in distilled water. The pH of the solution was maintained at 4.7 with drop wise addition of concentrated sulphuric acid. The metal sulphate solution was then heated at 80 °C for 2 h. Ammonium oxalate solution was added into the metal sulphate solution with constant stirring until the completion of precipitation. The chemical reactions can be given as

$$NiSO_4 + 2H_2O + C_2O_4^{2--} \rightarrow NiC_2O_4 2H_2O + SO_4^{2--}$$

* Corresponding author. Fax: +91 2342 224094.
E-mail address: pshindetj@yahoo.co.in (T.J. Shinde).

0925-8388/$ – see front matter © 2011 Elsevier B.V. All rights reserved.
doi:10.1016/j.jallcom.2011.10.001

$$NdSO_4 + 2H_2O + C_2O_4^{2--} \rightarrow NdC_2O_4 2H_2O + SO_4^{2--}$$

$$2FeSO_4 + 2H_2O + C_2O_4^{2--} \rightarrow Fe_2C_2O_4 2H_2O + 2SO_4^{2--}$$

The resultant precipitate was the mixture of solid solution of nickel oxalate, ferrous oxalate and neodymium oxalate. The precipitate was filtered and washed thoroughly with distilled water in order to remove the sulphate ions. The removal of sulphate ions was confirmed by barium chloride test. The precipitate was dried and presintered at 600 °C for 1 h. The presintered powders were milled in an agate mortar with acetone base and sintered in alumina crucibles at 1000 °C for 4 h. The sintered powders were milled again and mixed with an appropriate amount of 2 wt% polyvinyl alcohol and pressed into pellets of 1.3 cm diameter at a pressure of 7 dyne/cm^2. The pellets were finally sintered at 1000 °C for 4 h.

The X-ray diffraction (XRD) patterns of sintered powder were recorded on the Phillips make PW 3710 powder diffractometer using Cu-Kα radiations. Infrared (IR) absorption spectra of the samples were recorded on Perkin Elemer FT-IR spectrum one spectrometer in the frequency range 350–800 cm^{-1}. The scanning electron microphotographs of the samples were obtained on scanning electron microscope (SEM) model JEOL-JSM-6360. Physical densities of all the samples were measured by using Archimedes principle.

DC resistivity measurement of all the samples was carried out by two probe method in the temperature range 300–800 K. The saturation magnetization and hystersis parameters of the pelletized samples were measured at room temperature using high field loop tracer operating at 230 V, 50 Hz mains frequency. Curie temperature of all the sintered pellets was measured by using modified Loria Sinha technique.

3. Results and discussion

3.1. X-ray diffraction

The X-ray diffractograms of $NiNd_xFe_{2-x}O_4$ ($x = 0, 0.01, 0.02, 0.03$) system are presented in Fig. 1. The presence of (2 2 0), (3 1 1), (2 2 2), (4 0 0), (4 2 2), (5 1 1), (4 4 0) and (5 3 3) planes in the diffraction patterns confirms the formation of cubic spinel structure of all the samples. It is also observed that the peak intensity of Nd^{3+} substituted nickel ferrites is higher than that of nickel ferrites indicating strong crystallite structure corresponding to an increased homogeneity of the samples [30]. The lattice constant '*a*' of all the samples was calculated by using the formula [31],

$$a = d_{hkl}\sqrt{h^2 + k^2 + l^2} \quad (1)$$

where d_{hkl} is the observed interplaner distance for *hkl* planes.

The lattice constant of all the samples under investigation is presented in Table 1. The table shows that the lattice constant of all the samples increases with increase in Nd^{3+} content obeying Vegard's law. This can be explained on the basis of relative ionic radii of Fe^{3+} and Nd^{3+} ions. Since Fe^{3+} ions have smaller ionic radius (0.67 Å) than those of Nd^{3+} ions (1.07 Å), a partial replacement of the former by the later causes the increase in ionic radii on B-site. We [32] have reported that the lattice constant of $Ni_{0.6}Zn_{0.4}Nd_yFe_{2-y}O_4$ ($y = 0$, 0.01, 0.02 and 0.03) system increases with increase in Nd^{3+} content. Vermenko et al. [33] reported similar behavior for Nd^{3+} ($x \leq 0.03$) substituted nickel ferrites prepared by hydroxide method. Increase in lattice constant with increase in Dy^{3+} and Gd^{3+} content in nickel ferrites is also reported by Bharathi et al. [25,26]. Xiufeng et al. [34] reported that the lattice constant increases with increase in Nd^{3+} content in Ni–Zn ferrites. Samy [30] observed higher lattice constant for Nd^{3+} substituted Cu–Zn ferrite than unsubstituted one. The obtained value of the lattice parameter for nickel ferrite is in good agreement with that reported values [35,36].

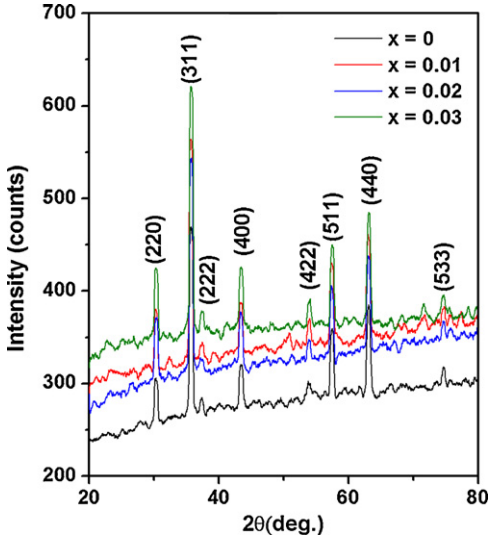

Fig. 1. X-ray diffraction patterns of $NiNd_xFe_{2-x}O_4$ system.

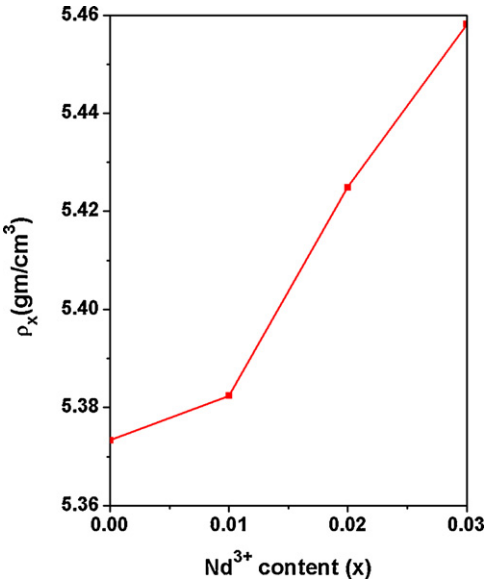

Fig. 2. Variation of X-ray density with Nd^{3+} content of $NiNd_xFe_{2-x}O_4$ system.

X-ray density (ρ_x) of all the samples was calculated by using relation [7],

$$\rho_x = \frac{8M}{Na^3} \quad (2)$$

where *M* is the molecular weight of the sample, *N* is the Avogadro's number (6.02×10^{23}).

The variation of X-ray density with Nd^{3+} content of $NiNd_xFe_{2-x}O_4$ ($x = 0$, 0.01, 0.02, 0.03) system is presented in Fig. 2. From this figure, it is seen that the X-ray density increases with increase in Nd^{3+} content, suggesting the increase in mass overtaking the increase in volume of the unit cell [32]. Physical density (ρ_p) of all the samples measured with Archimedes principle lies in the range of 5.07–5.28 g/cm^3. This is 98% to that of its theoretical values.

Porosity (*p*) of the samples was estimated by using formula [7],

$$p = 1 - \frac{\rho_p}{\rho_x} \quad (3)$$

Variation of physical density (ρ_p) and porosity (*p*) with Nd^{3+} content of $NiNd_xFe_{2-x}O_4$ ($x = 0$, 0.01, 0.02, 0.03) system is presented in Fig. 3. From this figure it is observed that the trends of physical density and porosity are opposite to each other.

Bond lengths (A–O and B–O) and ionic radii (r_A and r_B) on A-sites and B-sites of all the samples were calculated by using the relations [37].

$$A\text{–}O = \left(u - \frac{1}{4}\right) a\sqrt{3} \quad (4)$$

Table 1
Lattice constant (a), crystallite size (D), grain size (Ga) bond lengths (A–O and B–O) ionic radii (r_A and r_B) and absorption band (υ_1 and υ_2) on A-site and B-site of $NiNd_xFe_{2-x}O_4$ (x = 0, 0.01, 0.02, 0.03) system.

Nd^{3+} content x	Lattice constant a (Å)	Crystallite size D (nm)	Grain size Ga (μm)	Bond length (Å)		Ionic radii (Å)		Absorption bands (cm^{-1})	
				A–O site	B–O site	r_A	r_B	υ_1	υ_2
0	8.338	30.51	0.492	1.892	2.035	0.542	0.684	595	399
0.01	8.344	30.20	0.388	1.893	2.036	0.543	0.686	591	410
0.02	8.346	29.78	0.380	1.893	2.036	0.543	0.686	588	403
0.03	8.353	30.95	0.380	1.895	2.038	0.545	0.688	590	406

$$B\text{–}O = \left(\frac{5}{8} - u\right) a \quad (5)$$

$$r_A = \left(u - \frac{1}{4}\right) a\sqrt{3} - R_o \quad (6)$$

$$r_B = \left(\frac{5}{8} - u\right) a - R_o \quad (7)$$

where u is the oxygen ion parameter (0.381 Å), R_o is the radius of oxygen ion (1.32 Å).

The calculated values of bond lengths and ionic radii on A- and B-sites are presented in Table 1. From this table, it is noticed that, the bond lengths (B–O) and the ionic radii (r_B) on B-sites slightly increase with increase in Nd^{3+} content, whereas bond length (A–O) and ionic radii (r_A) on A-sites remain constant. This is attributed to smaller ionic radius of Fe^{3+} ion replaced by larger ionic radius of Nd^{3+} ion on B-site. It is observed that the ionic radii on A-site are less than that of B-site. This may be due to occupancy of Fe^{3+} ions (0.67 Å) on A-sites and Ni^{2+} ions (0.74 Å) and Nd^{3+} ions (1.07 Å) on B-sites [32,38].

The average crystallite size of the samples was calculated by using the Debye–Scherrer formula [39] and is presented in Table 1. It is observed that the crystallite size of the samples lies in the range 29.8–31 nm.

3.2. Infrared absorption spectra

The infrared absorption spectra of $NiNd_xFe_{2-x}O_4$ (x = 0, 0.01, 0.02, 0.03) system presented in Fig. 4 show two absorption bands in the range of 400–600 cm^{-1}. The higher wave number absorption band υ_1 is in the range of 595–588 cm^{-1} and the lower wave number absorption band υ_2 is in the range of 399–410 cm^{-1}. These bands are the common features of all the ferrites [40]. The band positions of υ_1 and υ_2 of all the samples are listed in Table 1. It is found that the absorption band υ_2 shifts slightly to higher wave number side and υ_1 shifts to lower wave number side with increase in Nd^{3+}content respectively. Similar type of variation in band positions is reported by Hemeda et al. [41] for rare earth substituted orthoferrites. The shifts in the bands υ_1 and υ_2 are due to the perturbation occurring in the Fe^{3+}–O^{2-} bond by substituting Nd^{3+} ions. From Fig. 4, it is also observed that the width of absorption bands of Nd^{3+} substituted nickel ferrites are smaller as compared to nickel ferrite, suggesting the occupancy of Nd^{3+} ions on octahedral B-sites.

3.3. Scanning electron microscopy

The scanning electron microphotographs of $NiNd_xFe_{2-x}O_4$ (x = 0, 0.01, 0.02, 0.03) system are presented in Fig. 5. The average grain size of all the samples under investigation was calculated by using the linear intercept method [42] and is presented in Table 1. It is found that the grain size of the samples decreases with increase in Nd^{3+} content. We [32,38] reported similar result for $Ni_{0.6}Zn_{0.4}Nd_yFe_{2-y}O_4$ (y = 0, 0.01, 0.02 and 0.03) and $ZnNd_yF_{2-y}O_4$ (y = 0, 0.01, 0.02, and 0.03) system. Recently [43–45] it is reported that the grain size of Mg–Cd ferrites decreases with increase in rare earth ions (La^{3+}, Sm^{3+} and Y^{3+}). Costa et al. [46] also observed similar results for Sm^{3+} substituted Ni–Zn ferrites.

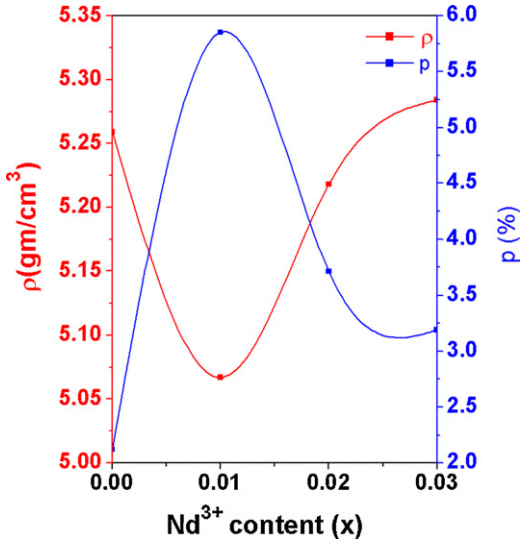

Fig. 3. Variation of physical density (ρ) and porosity (p) with Nd^{3+} content of $NiNd_xFe_{2-x}O_4$ system.

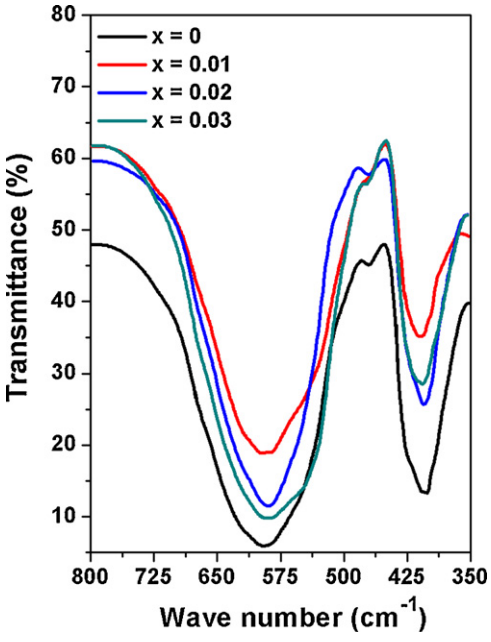

Fig. 4. Infrared absorption spectra of $NiNd_xFe_{2-x}O_4$ system.

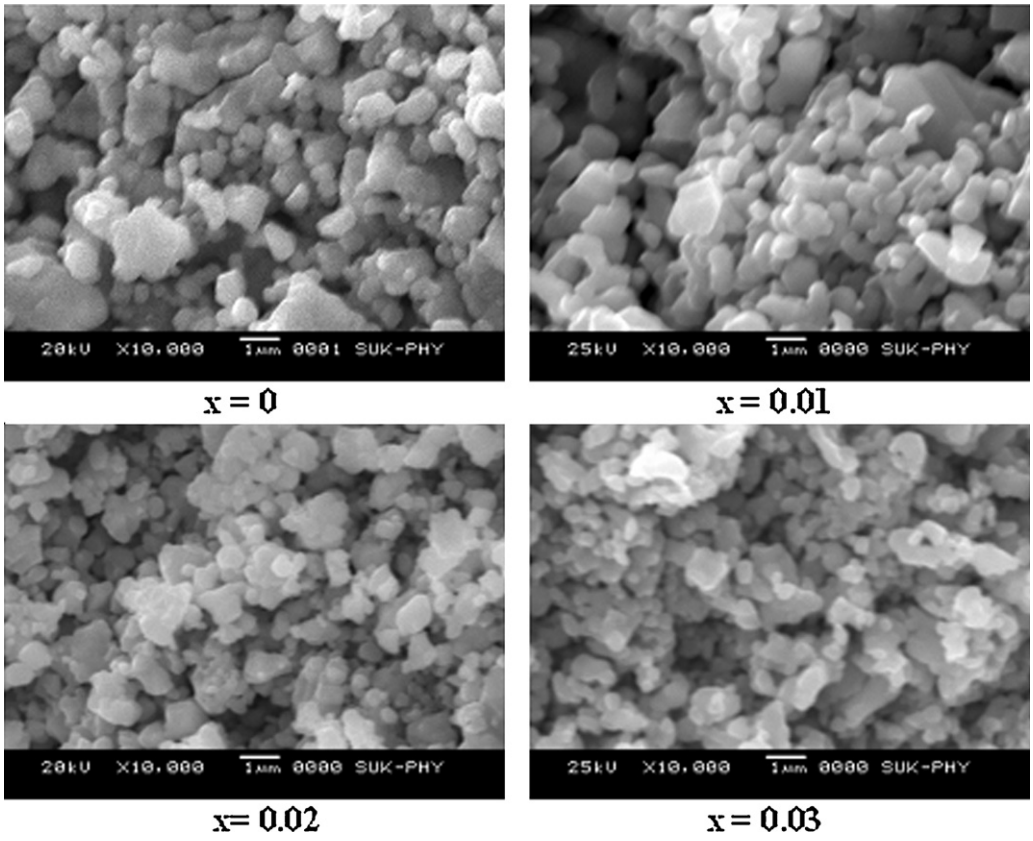

Fig. 5. Microphotographs of $NiNd_xFe_{2-x}O_4$ system.

3.4. DC electrical resistivity

The variation of DC electrical resistivity ($\log \rho$) against reciprocal of temperature ($10^3/T$) for $NiNd_xFe_{2-x}O_4$ ($x = 0$, 0.01, 0.02, 0.03) system is shown in Fig. 6. It is found that the resistivity of all the samples decreases with increasing temperature, indicating the semiconducting behavior of ferrites and follows Arrhenius relation,

$$\rho = \rho_0 e^{(\Delta E/kT)} \quad (8)$$

where

ρ_0 is the resistivity at room temperature,
k is the Boltzman constant (8.617×10^{-5} eV K^{-1}),
ΔE is the activation energy and
T is the absolute temperature.

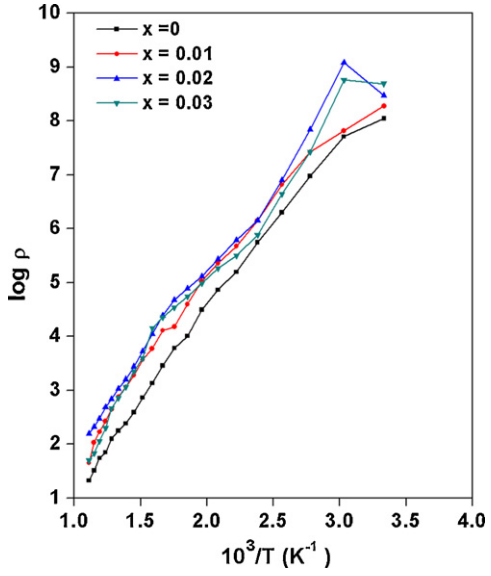

Fig. 6. Variation of $\log \rho$ against ($10^3/T$) for $NiNd_xFe_{2-x}O_4$ system.

From Fig. 6, it is further observed that, there are three regions with two breaks. The first region is due to impurities in materials at lower temperature [47–49]. The second region is a ferrimagnetic region with a break at Curie temperature (T_c) and third region is a paramagnetic region at higher temperature. Similar behavior is also observed by Said et al. [50] for Sm^{3+} substituted Ni–Cd ferrites. It is also observed that the resistivity of Nd^{3+} substituted nickel ferrites is higher than nickel ferrite. It is attributed to decreasing grain size with increase in Nd^{3+} content. Small grains imply larger number of insulating grain boundaries and hence greater energy barriers to electron conduction thereby resulting in higher resistivity [38,51]. The conduction in Nd^{3+} substituted nickel ferrites is due to hopping of electrons between Fe^{2+} and Fe^{3+} ions [52] and hole transfer from Ni^{3+} to Ni^{2+} ions. It is reported that Fe^{3+} ions partially occupy the A and B sites whereas Nd^{3+} and Ni^{2+} ions prefer the occupation of octahedral (B) sites [32]. On increasing Nd^{3+}content, the Fe^{3+} ion concentration on B-site decreases thereby decreasing the number of Fe^{2+} and Fe^{3+} ions responsible for electric conduction in ferrites on B-sites. This results in increasing resistivity with increase in Nd^{3+} content. In these ferrites, another reason for increase in resistivity on increasing Nd^{3+} content is that, the Nd^{3+} ions in B-site do not participate in the conduction processes due to their stable valency [53]. Recently we [38] reported that the resistivity of Nd^{3+} substituted zinc ferrites increases with increase in Nd^{3+} content. We [54,55] also observe higher resistivity for rare earth (La^{3+}, Y^{3+}

Table 2
Magnetization parameters, Curie temperatures and activation energies of $NiNd_xFe_{2-x}O_4$ system.

Nd^{3+} content x	Saturation magnetization M_s (emu/g)	Remenant magnetization M_r (emu/g)	Coercive force H_c (Oe)	Curie temperature T_c (°C)		Activation energy (eV)	
				Loria Sinha tech.	Resistivity plot	Para magnetic region	Ferro magnetic region
0	50.9	8.25	151	536	538	1.0914	0.7689
0.01	51.8	6.33	109	534	537	1.2403	0.8066
0.02	52	7.71	149	533	536	0.8644	0.6614
0.03	59.8	7.7	99	530	532	1.1244	0.9525

and Sm^{3+}) added magnesium and cadmium ferrites compared to unsubstituted one.

The activation energies of the samples were calculated for both ferrimagnetic (ΔE_f) and paramagnetic (ΔE_p) regions from the slopes of log ρ against $10^3/T$ plots and is presented in Table 2. It is found that the activation energy in ferrimagnetic region is less than that in paramagnetic region for all the samples. This can be attributed to the effect of magnetic ordering in the conduction process [56–58]. The change in activation energy with neodymium content is attributed to corresponding change in resistivity.

Curie temperature of all the samples observed from plots of log ρ versus $10^3/T$ and modified Loria Sinha technique are presented in Table 2. It is found that the Curie temperature of all the samples decreases with increase in Nd^{3+} content. This is attributed to weaker Nd–Fe interaction than Fe–Fe interaction for Nd^{3+} substitution. Such reduction in Curie temperature due to Nd^{3+} and rare earth ions (R = Yb, Er, Sm, Tb, Gd, Dy and Ce) substitution in Mg–Zn and Ni–Zn ferrites is reported [59,60]. Bharathi et al. [25] reported that the substitution of Dy for Fe causes a decrease in Curie temperature of the nickel ferrite. They attributed it to stronger Fe–Fe interaction than Fe–Dy interaction.

3.5. Saturation magnetization

Magnetic hysteresis curves for $NiNd_xFe_{2-x}O_4$ (x = 0, 0.01, 0.02 and 0.03) system are presented in Fig. 7. The magnetization parameters such as saturation magnetization (M_s), remenant magnetization (M_r) and coercive force (H_c) are presented in Table 2. It is observed that the saturation magnetization of the samples increases with increasing Nd^{3+} content. This is due to enhancing effect on the inter-sublattice exchange energy between Ni–O–Nd and Ni–O–Fe with respect to the Fe–O–Fe interaction in the ferrite lattice [32]. Similar result is reported by Upadhyay et al. [61] for Gd^{3+} substituted ferrite and Rezlescu et al. [62] for Gd^{3+} and Er^{3+} substituted Ni–Zn ferrite. Sudden increase in M_s for x = 0.03 composition is due to its larger crystallite size as compared to other samples. Since the energy of a magnetic particle in an external field is proportional to its crystallite size and the number of magnetic particles in a single magnetic domain, the larger the crystallite size, higher the saturation magnetization [63]. The behavior of H_c could be explained by Brown's relation [64] given by

$$H_c = \frac{2K_1}{\mu_o M_s} \quad (9)$$

where

K_1 is the anisotropy constant and
μ_o is the vacuum permeability

According to this relation H_c is inversely proportional to M_s, which is observed in present study. H_c and M_r of Nd^{3+} substituted ferrites are lower than unsubstituted ferrites. Similar result is reported by Zhao et al. [53] for RE^{3+} (La^{3+}, Nd^{3+}, Gd^{3+}) doped Ni–Mn ferrite calcined at 800 °C.

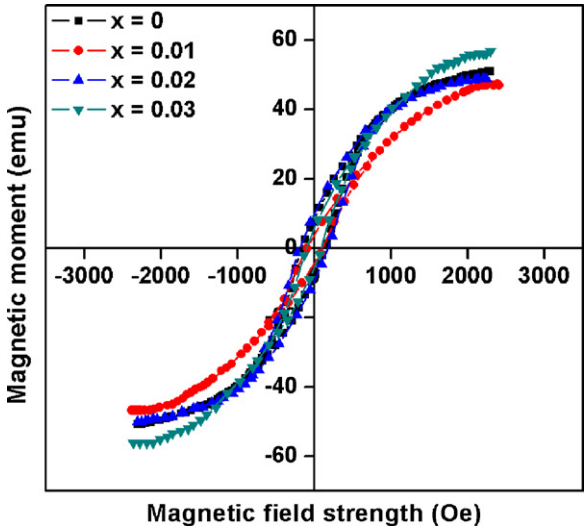

Fig. 7. Magnetic hysteresis curves for $NiNd_xFe_{2-x}O_4$ (x = 0, 0.01, 0.02 and 0.03) system.

4. Conclusions

Nanocrystalline Nd^{3+} substituted nickel ferrites were successfully synthesized by oxalate co-precipitation method. The lattice constant, in this ferrite is found to increase with increase in Nd^{3+} content. Crystallite size of the samples lies in the range 29.8–31 nm. The IR analysis shows the occupancy of Nd^{3+} ions on B-site. The grain size of the samples is found to decrease with increase in Nd^{3+} content. DC resistivity of Nd^{3+} substituted nickel ferrites is lower than nickel ferrites. It is found that, Curie temperature of the nickel ferrite decreases whereas saturation magnetization increases with increasing Nd^{3+} content.

References

[1] A. More, V.M.S. Verenkar, S.C. Mojumdar, J. Therm. Anal. Calorim. 94 (1) (2008) 63–67.
[2] L.C. Ping, L.M. Wei, C. Zhong, H. Juan-Ru, T. Yi-Ling, L. Tong, M. Wen-Bo, J. Mater. Sci. 42 (2007) 6133–6138.
[3] B.P. Rao, K.H. Rao, T.V. Rao, A. Paduraru, O.F. Caltun, J. Optoelectron. Adv. Phys. 7 (2) (2005) 701–704.
[4] P. Pramanik, A. Pathak, Bull. Mater. Sci. 17 (1994) 967–975.
[5] W. Li, F.-s. Li, Chin. Phys. B 17 (2008) 1858–1862.
[6] L. Zhao, H. Yang, L. Lei, J. Mater. Sci. Mater. Electron. 19 (2008) 992–995.
[7] T.J. Shinde, A.B. Gadkari, P.N. Vasambekar, Mater. Chem. Phys. 111 (2008) 87–91.
[8] M.M. Rashad, R.M. Mohamed, H. El-Shall, J. Mater. Process. Technol. 198 (2008) 139–146.
[9] J.M. Yang, F.S. Yen, J. Alloys Compd. 450 (2008) 387–394.
[10] C. Hu, Z. Gao, X. Yang, J. Magn. Magn. Mater. 320 (2008) L70–L73.
[11] S. Calvin, M.D. Shultz, L. Glowzenski, E.E. Carpenter, J. Undergrad. Res. (2008) 1–12.
[12] D.S. Mathew, R.S. Juang, Chem. Eng. J. 129 (2007) 51–65.
[13] S.K. Sharma, R. Kumar, S. Kumar, M. Knobel, C.T. Meneses, V.V. Kumar Siva, V.R. Reddy, M. Singh, C.G. Lee, J. Phys.: Condens. Matter 20 (2008) 235214–235221.
[14] P.Y. Lee, K. Ishizaka, H. Suematsu, W. Jiang, K. Yatsui, J. Nanopart. Res. 8 (2006) 29–35.

[15] A.M. Gismelseed, A.A. Yousif, Physica B 370 (2005) 215–222.
[16] H.N. Pandya, R.G. Kulkarni, Solid State Commun. 61 (1987) 645–647.
[17] T.J. Shinde, B.P. Ladgaonkar, B.J. Nalawade, M.A. Anuse, P.N. Vasambekar, A.S. Vaingankar, Proc. Solid State Phys. Symp. 42 (1999) 575–576.
[18] J.T.E. Galindo, A.H. Adair, C.E. Botez, V.C. Flores, D.B. Baques, L.F. Cobas, J.A.M. Aquino, Appl. Phys. A87 (2007) 743–747.
[19] A.T. Raghavender, D. Pajic, K. Zadro, T. Milekovic, P.V. Rao, K.M. Jadhav, d D. Ravinder, J. Magn. Magn. Mater. 316 (2007) 1–7.
[20] K.M. Batoo, S. Kumar, C.G. Lee, Alimuddin, Curr. Appl. Phys. 9 (4) (2009) 826–832.
[21] S.S. Bhatu, Y.K. Lakhani, A.R. Tanna, N.H. Vasoya, J.U. Buch, P.U. Sharma, U.N. Trivedi, H.H. Joshi, K.B. Modi, Indian J. Pure Appl. Phys. 45 (2007) 596–608.
[22] K. Roumaih, J. Alloys Compd. 465 (2008) 291–295.
[23] V.K. Mittal, P. Chandramohan, S. Bera, M.P. Srinivasan, S. Velmurugan, S.V. Narasimhan, Solid State Commun. 137 (1–2) (2006) 6–10.
[24] H. Yang, L. Zhao, X. Yang, L. Shen, L. Yu, W. Sun, Y. Yan, W. Wang, S. Feng, J. Magn. Magn. Mater. 271 (2–3) (2004) 230–236.
[25] K.K. Bharathia, J.A. Chelvaneb, G. Markandeyulu, J. Magn. Magn. Mater. 321 (22) (2009) 3677–3680.
[26] K.K. Bharathi, G. Markandeyulu, J. Appl. Phys. 103 (2008), 07E309-1–07E309-2.
[27] N. Rezlescu, E. Rezlescu, C. Pasnicu, M.L. Craus, J. Phys.: Condens. Matter 6 (1994) 5707–5716.
[28] Y.M. Al Angari, J. Magn. Magn. Mater. 323 (2011) 1835–1839.
[29] M. Ishaque, M.U. Islama, M. Azhar Khan, I.Z. Rahman, A. Genson, S. Hampshire, J. Phys.: Condens. Matter 405 (6) (2010) 1532–1540.
[30] A.M. Samy, J. Mater. Eng. Perform. 12 (5) (2003) 569–572.
[31] B.D. Culity, Elements of X-ray Diffraction, Addison Wesley Pub Co INC, 1956.
[32] T.J. Shinde, A.B. Gadkari, P.N. Vasambekar, J. Mater. Sci. Mater. Electron. 21 (2010) 120–124.
[33] L.A. Vermenko, T.Y. Gridasova, E.N. Lukachina, Consultants Bureau, Division of Plenum Publishing Corporation, New York, 1974, pp. 732–735.
[34] F. Xiufeng, R. Huping, Z. Yanghuan, G. Shihai, W. Xinlin, Rare Metals 27 (3) (2008) 287–291.
[35] X.F. Zhu, L.F. Chen, J. Magn. Magn. Mater. 323 (2011) 3138–3142.
[36] K.K. Bharathi, K. Balamurugan, P.N. Santhosh, M. Pattabiraman, G. Markandeyulu, Phys. Rev. B 77 (2008) 172401–172404.
[37] K.J. Standley, Oxide Magnetic Materials, Clarodon Press, Oxford, 1972.
[38] T.J. Shinde, A.B. Gadkari, P.N. Vasambekar, J. Magn. Magn. Mater. 322 (2010) 2777–2781.
[39] H.P. Klug, L.E. Alexander, X-ray Diffraction Procedure, Wiley INC, New York, 1954.
[40] R.D. Waldron, Phys. Rev. B 99 (1955) 1727–1735.
[41] O.M. Hemeda, M.M. Barakat, D.M. Hemeda, Turk. J. Phys. 27 (2007) 537–549.
[42] J.C. Warst, J.A. Nelson, J. Am. Ceram. Soc. 55 (1972) 109–112.
[43] A.B. Gadkari, T.J. Shinde, P.N. Vasambekar, Rare Metals 29 (2) (2010) 168–173.
[44] A.B. Gadkari, T.J. Shinde, P.N. Vasambekar, Mater. Charact. 60 (2009) 1328–1333.
[45] A.B. Gadkari, T.J. Shinde, P.N. Vasambekar, Mater. Chem. Phys. 114 (2009) 505–510.
[46] A.C.F.M. Costa, M.R. Morelli, R.H.G.A. Kiminami Mi, J. Mater. Sci. 39 (5) (2004) 1723–1728.
[47] M.G. Patil, V.C. Mahajan, S.D. Lotke, B.V. Bhise, S.A. Patil, Solid State Commun. 91 (8) (1994) 667–670.
[48] B.L. Patil, S.R. Sawant, S.A. Patil, R.N. Patil, J. Mater. Sci. 29 (1994) 175–178.
[49] B.V. Bhise, S.D. Lotke, S.A. Patil, Phys. Stat. Sol. (a) 157 (2) (1996) 411–419.
[50] M.Z. Said, D.M. Hemeda, S.A. Kadar, G.Z. Farag, Turk. J. Phys. 31 (2007) 41–50.
[51] A. Verma, D.C. Dube, J. Am. Ceram. Soc. 88 (3) (2005) 519–523.
[52] J. Smit, H.P.J. Wijn, Ferrites, Philips Technical Library, Eindhoven, The Netherlands, 1956, p. 230.
[53] L. Zhao, H. Yang, L. Yu, Y. Cui, X. Zhao, S. Feng, J. Mater. Sci. 42 (2007) 686–691.
[54] P.N. Vasambekar, A.B. Gadkari, T.J. Shinde, Proc. 54th DAE Solid State Phys. Sym, vol. 54, 2009, pp. 1081–1082.
[55] A.B. Gadkari, P.N. Vasambekar, T.J. Shinde, Proc. 54th DAE Solid State Phys. Sym, vol. 54, 2009, pp. 1099–1100.
[56] M.A. Gabal, Y.M. Al Angari, Mater. Chem. Phys. 115 (2009) 578–584.
[57] B.K. Bammannavar, L.R. Naik, R.B. Pujar, Prog. Electromagn. Res. Lett. 4 (2008) 121–129.
[58] K.V. Kumar, D. Ravinder, Mater. Lett. 52 (2002) 166–168.
[59] B.P. Ladgaonkar, P.N. Vasambekar, A.S. Vaingankar, J. Shivaji Univ. (Sci.) 36 (1999) 49–57.
[60] N. Rezlescu, E. Rezlescu, Solid State Commun. 88 (2) (1993) 139–141.
[61] R.V. Upadhyay, R.V. Mehta, K. Parekh, D. Srinivas, R.P. Pant, J. Magn. Magn. Mater. 201 (1999) 129–132.
[62] N. Rezlescu, E. Rezlescu, C. Pasnicu, M.L. Craus, J. Magn. Magn. Mater. 136 (1994) 319–326.
[63] X. Juna, S. Xiangqiana, Z. Yongwei, Rare Metals 28 (2) (2009) 151–155.
[64] J.M.D. Coey, Rare Earth Permanent Magnetism, John Wiley and Sons, New York, 1996, p. 220.